Numerical simulation of Lugiato-Lefever equation for Kerr combs generation in Fabry-Perot resonators

Mouhamad Al Sayed Ali, Stéphane Balac, Gabriel Caloz, Monique Dauge, Fabrice Mahé, Germain Bourcier, Arnaud Fernandez, Olivier Llopis

Numerical simulation of Lugiato-Lefever equation for Kerr combs generation in Fabry-Perot resonators

Mouhamad Al Sayed Ali, Stéphane Balac,* Gabriel Caloz, Monique Dauge, and Fabrice Mahé
UNIV. RENNES, CNRS, IRMAR - UMR 6625, F-35000 Rennes, France

Germain Bourcier, Arnaud Fernandez, and Olivier Llopis
LAAS-CNRS, Université de Toulouse, CNRS, UPS, Toulouse, France

Lugiato-Lefever equation (LLE) is a nonlinear Schrödinger equation with damping, detuning and driving terms, introduced as a model for Kerr combs generation in ring-shape resonators and more recently, in the form of a variant, in Fabry-Perot (FP) resonators. The aim of this paper is to present some numerical methods that complement each other to solve the LLE in its general form both in the dynamic and in the steady state regimes. We also provide some mathematical properties of the LLE likely to help the understanding and interpretation of the numerical simulation results.

I. INTRODUCTION

Kerr frequency combs refer to a laser source whose spectrum consists of a series of discrete, equally spaced frequency lines, which are generated in an optical cavity from a pump laser by the Kerr nonlinearity. Applications of Kerr frequency combs are numerous in various domains in optics such as optical metrology, lidars or time-frequency systems. The coherent conversion of the pump laser to a frequency comb has been obtained in a variety of optical resonator such as whispering-gallery mode resonators (WGM), fiber ring resonators or integrated ring-resonators of high non-linearity [5; 6; 15; 18]. Here we are concerned with Fabry-Perot (FP) resonators formed by an optical fiber bounded at each end by a multi-layer dielectric mirror. Beyond their ease of design and manipulation [20] FP resonators allow a durable and reproducible coupling in all-fiber optical systems, enabling their use as a compact source of Kerr frequency combs. They are considered as an interesting alternative to crystalline WGM resonators and to integrated optical resonators.

An approach for the theoretical understanding of Kerr comb generation process in WGM resonators and integrated ring-resonators relies on a spatiotemporal partial differential equation referred to as the Lugiato–Lefever equation (LLE), which is a nonlinear Schrödinger equation with damping, detuning, and driving terms [16] that have been initially introduced in the late 80's by L. Lugiato and R. Lefever as a model for spontaneous pattern formation in nonlinear optical systems. More recently, this model has been extended to describe Kerr comb generation process in FP resonators in [7]. The difference between the original LLE for ring shaped (RS) resonators and the equation obtained as a model for Kerr frequency combs generation in a FP resonator lies on the one hand in the presence of an additional integral term that makes the equation non-local in space and on the other hand on the periodic boundary conditions resulting from the modeling approach of the dielectric mirrors at each end of the fiber. The LLE for a FP resonator (in short the FP-LLE) can be expressed as

$$\frac{\partial \psi}{\partial t}(\theta,t) = -\mathrm{i}\frac{\beta}{2}\frac{\partial^2 \psi}{\partial \theta^2}(\theta,t) - (1+\mathrm{i}\alpha)\,\psi(\theta,t) + \mathrm{i}\,\psi(\theta,t)\left(|\psi(\theta,t)|^2 + \frac{\sigma}{\pi}\int_{-\pi}^{\pi}|\psi(\zeta,t)|^2\,\mathrm{d}\zeta\right) + F \quad (1a)$$

where, in order to cover in a unified way the two above mentioned cases corresponding respectively to RS resonators [13] and FP resonators [7], we have introduced a normalized space variable $\theta \in]-\pi,\pi[$ and the parameter σ. In the case of a FP resonator with a cavity made from a fiber with length L, the space variable θ is related to the position z along the fiber by $\theta = \pi z/L$ whereas for a RS resonator θ refers to the polar coordinate. Moreover, (1a) with $\sigma = 0$ coincides with the original LLE for RS whereas for $\sigma = 1$ we have the specific LLE for FP resonators. The constant, unit-less and real valued parameters in (1a) are as follows:

- $F > 0$ is the amplitude of the continuous wave laser pump;
- β is the group velocity dispersion (GVD) parameter of the resonator; it can be either positive corresponding to the so-called *normal regime* or negative corresponding to the *anomalous regime*;
- α is the cavity phase detuning of the laser pump.

Equation (1a) is to be considered together with the following periodic boundary conditions:

$$\psi(-\pi,t) = \psi(\pi,t) \quad (1b)$$

$$\frac{\partial \psi}{\partial \theta}(-\pi,t) = \frac{\partial \psi}{\partial \theta}(\pi,t). \quad (1c)$$

Furthermore, an initial condition is also required:

$$\forall \theta \in [-\pi,\pi] \qquad \psi(\theta,t=0) = \psi_0(\theta) \quad (1d)$$

where ψ_0 is a given function that describes the state of the cavity at initial time $t = 0$. Throughout the paper,

* Corresponding author: stephane.balac@univ-rennes.fr

we will denote by $\|\ \|$ the $\mathbb{L}^2$ norm (a.k.a. energy norm) over $[-\pi,\pi]$ defined as

$$\|u\| = \Big(\int_{-\pi}^{\pi} |u(\zeta)|^2\ \mathrm{d}\zeta\Big)^{\frac{1}{2}}. \tag{2}$$

A comprehensive analysis of the way the FP-LLE can be justified from Maxwell equations is conducted in [2] and relies on different assumptions including the low transmission approximation, the high-Q limit regime approximation and the assumption that the electric field injected in the FP cavity is polarized in a direction $\mathbf{e_x}$ transverse to the propagation direction $\mathbf{e_z}$ (see also [24]). It is established in [2] that, up to a transformation introduced to handle simultaneously the forward and backward waves through a symmetrization on $[-L,L]$, the FP-LLE solution ψ is related to the slowly varying envelop of the forward E_F and backward E_B electric field wave propagating at a velocity v_g through the relations

$$E_F(z,t) = \sum_{n\in\mathbb{Z}} g_n(t) \exp\Big(\mathrm{i}\frac{\pi n}{L}\big(v_g t - z\big)\Big) \tag{3a}$$

$$E_B(z,t) = \sum_{n\in\mathbb{Z}} g_n(t) \exp\Big(\mathrm{i}\frac{\pi n}{L}\big(v_g t + z\big)\Big) \tag{3b}$$

where the $g_n(t), n\in\mathbb{Z}$, are the Fourier coefficients of ψ with respect to the space variable. The electric field component of light-wave in the FP-cavity is expressed $\forall z\in[0,L], \forall t\in\mathbb{R}$ as

$$\mathbf{E}(z,t) = \Big(E_F(z,t)\,\mathrm{e}^{\mathrm{i}\gamma z} + E_B(z,t)\,\mathrm{e}^{-\mathrm{i}\gamma z}\Big)\,\mathrm{e}^{-\mathrm{i}\omega_0 t}\ \mathbf{e_x} + \text{c.c.}$$

where ω_0 is the so-called *carrier frequency* of the electric field, γ is the mode propagation constant and *c.c.* means "complex conjugate".

Let us clarify the link between steady state solutions to the FP-LLE problem (1) and Kerr frequency combs. (A more physical description in the case of WGM disk resonator can be found e.g. in [13].) In the frequency domain, we have $\forall z\in[0,L], \forall\omega\in\mathbb{R}^+$

$$\widehat{\mathbf{E}}(z,\omega) = \Big(\widehat{E}_F(z,\omega_0-\omega)\,\mathrm{e}^{\mathrm{i}\gamma z} + \widehat{E}_B(z,\omega_0-\omega)\,\mathrm{e}^{-\mathrm{i}\gamma z}\Big)\,\mathbf{e_x} + \text{c.c.}$$

where $\widehat{\mathbf{E}}(z,\cdot)$ refers to the Fourier transform of $\mathbf{E}(z,\cdot)$. For steady state solutions ψ to FP-LLE, the sequence $(g_n)_{n\in\mathbb{Z}}$ is independent of time and it follows from (3) that

$$\widehat{E}_F(z,\omega_0-\omega) = \sum_{n\in\mathbb{Z}} g_n \mathrm{e}^{-\mathrm{i}\pi n z/L}\,\delta(\omega_0-\omega+\pi n\tfrac{v_g}{L})$$

$$\widehat{E}_B(z,\omega_0-\omega) = \sum_{n\in\mathbb{Z}} g_n \mathrm{e}^{\mathrm{i}\pi n z/L}\,\delta(\omega_0-\omega+\pi n\tfrac{v_g}{L})$$

where δ is the Dirac delta function. Thus, in the frequency domain, the electric field related to steady-state solutions ψ to the FP-LLE at the cavity end located at $z=L$ is a "comb" with equidistant frequencies ω at a distance $\frac{\pi v_g}{L}$ from each other and centered around the carrier frequency ω_0.

The goals of this paper are to give an overview of the mathematical properties of the solutions to the FP-LLE problem in connection with Kerr frequency combs generation and to propose some numerical methods enabling the investigation by numerical simulation of some features of these solutions, both in the time-dynamic regime and in the steady state regime. The study of FP-LLE solutions is not a simple problem and may conceal some pitfalls. This is reflected in the numerical simulations in various ways.

The paper is organized as follows. Section II is devoted to some mathematical properties of solutions to the FP-LLE. A particular attention is paid to steady state solutions that are the solutions of interest when studying Kerr frequency combs. In Section III we provide some numerical methods for solving the FP-LLE that each gives a different viewpoint when exploring the properties of FP-LLE solutions. Finally, in Section IV we show some results obtained by numerical simulation that illustrate the wealth of situations related to the FP-LLE. The paper is completed by two appendices. Although there is no energy conservation due to the non Hamiltonian structure of the LLE, in Appendix A an explicit bound of the energy is given. In Appendix B, explicit necessary conditions to have bifurcation points from constant solutions are given for both the FP-LLE and its discretization by finite differences.

II. OVERVIEW OF MATHEMATICAL PROPERTIES OF THE LLE MODEL

II.1. Properties of the time-dynamic FP-LLE problem

Let us first observe that a solution ψ to the FP-LLE problem (1) can be viewed as a 2π-periodic function defined on the real line $\mathbb{R}$. It follows that the function $\theta\in\mathbb{R}\mapsto\psi(\theta-c)$ for any $c\in\mathbb{R}$ provides a solution to problem (1). Thus, periodic boundary conditions imply a translation invariance of solutions. Moreover, we can also point out that periodic solutions to (1a) over $\mathbb{R}$ exhibit some dilation property with respect to β. Namely, let ψ be a 2π-periodic solution to (1a) and let $\varphi:\theta\in\mathbb{R}\mapsto\psi(p\theta)$ for a given $p\in\mathbb{N}^*$. One can easily deduce from (1a) that the $\frac{2\pi}{p}$-periodic function φ is such that

$$\frac{\partial\varphi}{\partial t}(\theta,t) = -\mathrm{i}\frac{\beta}{2p^2}\,\frac{\partial^2\varphi}{\partial\theta^2}(\theta,t) - (1+\mathrm{i}\alpha)\,\varphi(\theta,t) + \mathrm{i}\,\varphi(\theta,t)\Big(|\varphi(\theta,t)|^2 + p\,\frac{\sigma}{\pi}\int_{-\pi/p}^{\pi/p}|\varphi(\zeta,t)|^2\ \mathrm{d}\zeta\Big) + F.$$

and since φ is $\frac{2\pi}{p}$-periodic, we have

$$p\int_{-\pi/p}^{\pi/p}|\varphi(\zeta,t)|^2\ \mathrm{d}\zeta = \int_{-\pi}^{\pi}|\varphi(\zeta,t)|^2\ \mathrm{d}\zeta.$$

It follows that if we have a 2π-periodic solution ψ to the FP-LLE for a given value of β, then it generates thanks to a dilation transformation with factor p, a $2\pi/p$-periodic solution to the FP-LLE for a value of the parameter β divided by p^2.

Let us introduce the space of 2π-periodic functions $V = \{v \in \mathsf{H}^1_{\mathrm{loc}}(\mathbb{R})\ ;\ v(x-\pi) = v(x+\pi)\,\forall x \in \mathbb{R}\}$ where $\mathsf{H}^1_{\mathrm{loc}}(\mathbb{R})$ denotes the Sobolev space of functions that are square-integrable, as well as their first derivative, over every bounded interval. In the case $\sigma = 0$, we find in [11] that for every $\psi_0 \in V$ the Cauchy problem (1) possesses a unique solution $\psi \in \mathsf{L}^\infty(\mathbb{R}^+, V)$ and that for every $t \in \mathbb{R}^+$ the mapping $\psi_0 \mapsto \psi(\cdot, t)$ is continuous on V. Moreover, for every $t \in \mathbb{R}^+$, we have the energy estimate

$$\|\psi(\cdot,t)\|^2 \leq \mathrm{e}^{-t}\,\|\psi_0\|^2 + 2\pi F^2\,(1-\mathrm{e}^{-t}). \tag{4}$$

The full framework of [11] does not apply to the case $\sigma = 1$ due to the non-linear integral term. Nevertheless, by the same chain of arguments as in [11], one can show that the energy estimate (4) holds as well when $\sigma = 1$, see Appendix A.

II.2. Steady state solutions

As mentioned in the introduction, Kerr frequency combs are related to steady state solutions to the LLE problem (1). Such time independent solutions satisfy the following ordinary differential equation on $]-\pi,\pi[$ deduced from (1a)

$$-\mathrm{i}\frac{\beta}{2}\,\psi''(\theta) - (1+\mathrm{i}\alpha)\,\psi(\theta) + \mathrm{i}\;\psi(\theta)\left(|\psi(\theta)|^2 + \frac{\sigma}{\pi}\,\|\psi\|^2\right) + F = 0 \tag{5a}$$

together with the following boundary conditions:

$$\psi(-\pi) = \psi(\pi) \qquad \text{and} \qquad \psi'(-\pi) = \psi'(\pi). \tag{5b}$$

The mathematical study of the LLE (1) when $\sigma = 0$ has been the subject of several publications in the last decade. To our knowledge, the first mathematical investigation of the RS-LLE equation from a viewpoint of bifurcation theory from trivial constant solutions is [19]. A fairly complete numerical investigation of the various steady-state solutions to the RS-LLE equation has been undertaken in [12; 13] where a stability analysis is developed to obtain spatial bifurcation maps. Existence and stability of periodic solutions to the RS-LLE problem has been investigated in [10] using a center manifold reduction theory. This approach provides a detailed behavior of periodic solutions in a neighborhood of specific parameter values, but does not allow a global description of solutions when the RS-LLE parameters change. In [17] and [9] a bifurcation analysis for RS-LLE equation based on the bifurcation theorems of Crandall and Rabinowitz [8] is conducted. This approach provides a different and more global viewpoint than the one obtained by the center manifold reduction approach. Furthermore, in [17] the authors provide numerical computations of bifurcation diagrams in various emblematic cases which are very inspiring.

Remark 1. *Note that in the steady state regime, given a solution ψ to the LLE equation (5a) for $\sigma = 1$, the quantity $\alpha_\psi = \frac{1}{\pi}\|\psi\|^2$ is a constant and therefore equation (5a) can be recast in the following way*

$$-\mathrm{i}\frac{\beta}{2}\,\psi''(\theta) - (1+\mathrm{i}(\alpha-\alpha_\psi))\,\psi(\theta) + \mathrm{i}\;\psi(\theta)\,|\psi(\theta)|^2 + F = 0.$$

The LLE for FP resonators ($\sigma = 1$) has the same expression as the LLE for a RS resonator ($\sigma = 0$) with a modified cavity phase detuning parameter.

From Remark 1 we can expect at first sight to have similar mathematical properties for solutions to the FP-LLE as the ones we have for the RS-LLE that have been extensively studied in the literature. However, we can not directly deduce the features of solutions to FP-LLE from known results to the RS-LLE since the change in the detuning parameter depends on the $\mathbb{L}^2$ norm of the solution and therefore is unknown and solution dependent. What we can claim is that each solution ψ to the FP-LLE for a given cavity phase detuning parameter α is also a solution to the RS-LLE for a different detuning parameter given by $\alpha - \frac{1}{\pi}\|\psi\|^2$.

Note that for a given set of parameters (β, α, F), one can exhibit up to three constant solutions (among others steady state solutions). These solutions are often referred to as *flat solutions*, see Section II.3 below. As a consequence, it is clear that the steady state problem (5) does not have a unique solution.

Finally, let us mention that problem (5) written for a complex valued unknown ψ can be set in an equivalent real valued form by considering separately real and imaginary parts. Namely, let u_1 denotes the real part of ψ and u_2 its imaginary part; We deduce from (5a) the following two differential equations satisfied by (u_1, u_2)

$$-\frac{\beta}{2}\,u_1'' - \alpha u_1 - u_2 + u_1\left(u_1^2 + u_2^2 + \frac{\sigma}{\pi}\,\mathcal{I}(u_1,u_2)\right) = 0 \tag{6a}$$

$$-\frac{\beta}{2}\,u_2'' + u_1 - \alpha\,u_2 + u_2\left(u_1^2 + u_2^2 + \frac{\sigma}{\pi}\,\mathcal{I}(u_1,u_2)\right) - F = 0 \tag{6b}$$

where

$$\mathcal{I}(u_1,u_2) = \int_{-\pi}^{\pi} (u_1^2(\zeta) + u_2^2(\zeta))\;\mathrm{d}\zeta = \|\psi\|^2. \tag{6c}$$

From (5b) we obtain the following periodic boundary conditions for $u_k, k = 1, 2$

$$u_k(-\pi) = u_k(\pi) \qquad \text{and} \qquad u_k'(-\pi) = u_k'(\pi). \tag{6d}$$

II.3. Flat solutions

A special kind of steady state solutions to the FP-LLE (1a) are solutions that depend neither on time nor on position. These trivial solutions are called *flat* solutions and they can be explicitly calculated as detailed below. From a practical viewpoint, their interest in the study of steady state solutions to the LLE is related to the practical observation, see Section IV, that stable spatially periodic solutions bifurcate from this set of solutions when the LLE parameters α or F vary. Moreover, these flat solutions behave as attractors when using numerical methods such as the Split-Step method or a Collocation method: Namely, a special attention has to be paid to the choice of the computational setting in order to get a solution other than a flat solution.

For a flat solution $\psi_\bullet$, the FP-LLE (1a) reads

$$(1+\mathrm{i}\alpha)\,\psi_\bullet - \mathrm{i}\,\psi_\bullet\left(|\psi_\bullet|^2+2\sigma|\psi_\bullet|^2\right) = F. \tag{7}$$

By taking into account the product of (7) by its conjugate, we deduce that

$$\left(1+(\alpha-(1+2\sigma)\rho_\bullet)^2\right)\rho_\bullet = F^2 \tag{8}$$

where we have set

$$\rho_\bullet = |\psi_\bullet|^2. \tag{9}$$

One may wonder how many flat solutions the FP-LLE (1a) holds. To answer the question we must determine how many *positive* solutions $\rho_\bullet$ equation (8) owns for a couple of parameters (α, F) fixed. Since $\rho_\bullet > 0$, we are interested in the positive roots of the polynomial $P \in \mathbb{R}[X]$ where

$$P \overset{\text{def}}{=} (1+2\sigma)^2\,X^3 - 2\alpha(1+2\sigma)\,X^2 + (1+\alpha^2)X - F^2. \tag{10}$$

As well known, P may have one real root or three real roots (counted with multiplicity); However, the number of positive roots may *a priori* vary from zero to three. Note that once $\rho_\bullet$ is known as one of the root of P, one can easily deduce the corresponding flat solution $\psi_\bullet$. From equation (7), we have

$$\psi_\bullet = \frac{F}{1+\mathrm{i}(\alpha-(1+2\sigma)\rho_\bullet)}. \tag{11}$$

To investigate existence of positive roots to P, let $G_\alpha : \mathbb{R} \to \mathbb{R}$ be the mapping defined for a fixed value of α considered as a parameter by

$$G_\alpha(\rho) = \left(1+(\alpha-(1+2\sigma)\rho)^2\right)\rho. \tag{12}$$

G_α is a degree 3 polynomial mapping with $G_\alpha(0) = 0$ and $\lim\limits_{\rho\to\pm\infty} G_\alpha(\rho) = \pm\infty$. Its derivative is given by

$$G'_\alpha(\rho) = 3(1+2\sigma)^2\,\rho^2 - 4\alpha(1+2\sigma)\,\rho + (1+\alpha^2) \tag{13}$$

and the discriminant of the binomial equation $G'_\alpha(\rho) = 0$ is $\Delta = 4(1+2\sigma)^2\,(\alpha^2-3)$. Thus, equation $G'_\alpha(\rho) = 0$ has two conjugate complex roots when $\alpha^2 < 3$, one real root when $\alpha^2 = 3$ and two real roots when $\alpha^2 > 3$. It follows that G_α is a strictly increasing function over $\mathbb{R}$ when $\alpha^2 \leq 3$. Since $G_\alpha(0) = 0$, it defines a one-to-one mapping from $[0,+\infty[$ onto $[0,+\infty[$ and we can conclude that when $\alpha^2 \leq 3$ equation (8) has a unique positive solution.

The case when $\alpha^2 > 3$ is less straightforward. Solving equation $G'_\alpha(\rho) = 0$, we find that G_α has two local extrema located at

$$\rho_\pm = \frac{2\alpha \pm \sqrt{\alpha^2-3}}{3(1+2\sigma)}. \tag{14}$$

Moreover, one can easily check that when α is positive, the two local extrema abscissas $\rho_\pm$ are positive with $0 < \rho_- < \rho_+$ and that when α is negative $\rho_- < \rho_+ < 0$. Thus, when α is negative, G_α is strictly increasing over $[0,+\infty[$. Since $G_\alpha(0) = 0$, it defines a one-to-one mapping from $[0,+\infty[$ onto $[0,+\infty[$ and we conclude that when $\alpha < -\sqrt{3}$ equation (8) has a unique positive solution.

Finally, it remains to consider the case when $\alpha > \sqrt{3}$ where G_α increases from 0 to ρ_-, then decreases from ρ_- to ρ_+ and finally increases from ρ_+ to infinity. We have

$$G_\alpha(\rho_+) = \frac{2\,\alpha+\sqrt{\alpha^2-3}}{27(1+2\sigma)}\left(9+\left(\alpha-\sqrt{\alpha^2-3}\right)^2\right)$$
$$G_\alpha(\rho_-) = \frac{2\,\alpha-\sqrt{\alpha^2-3}}{27(1+2\sigma)}\left(9+\left(\alpha+\sqrt{\alpha^2-3}\right)^2\right)$$

and for $\alpha > \sqrt{3}$ these two quantities are positives. It follows that

- when $F^2 \in]G_\alpha(\rho_+), G_\alpha(\rho_-)[$, equation (8) has a three positive solutions;
- when $F^2 = G_\alpha(\rho_+)$ or when $F^2 = G_\alpha(\rho_-)$, equation (8) has a two positive solutions;
- when $F^2 < G_\alpha(\rho_+)$ or when $F^2 > G_\alpha(\rho_-)$, equation (8) has a unique positive solution.

Note that when there exist three positive solutions ρ_1, ρ_2, ρ_3 to equation (8), they can be arranged in increasing order as follows

$$0 < \rho_1 < \rho_- < \rho_2 < \rho_+ < \rho_3. \tag{15}$$

We have depicted in Fig. 1 the plane (α, F^2) and we have indicated the different areas corresponding to the number of solutions to equation (8) when $\sigma = 1$. One can note that flat solutions do not depend on the value of the parameter β. We have also depicted in Fig. 2 the variation of $\rho_\bullet = |\psi_\bullet|^2$ as a function of F for $\alpha \in \{1,5,10,15\}$. For a fixed value of F and $\alpha \in \{5,10,15\}$, one can see that one may have 1, 2 or 3 corresponding values for $\rho_\bullet$ (intersection of the curves with the vertical line passing through $(F,0)$ whereas for $\alpha = 1$, we have only one values for $\rho_\bullet$ whatever is the value of F. A similar observation can be done in Fig. 3 where we have

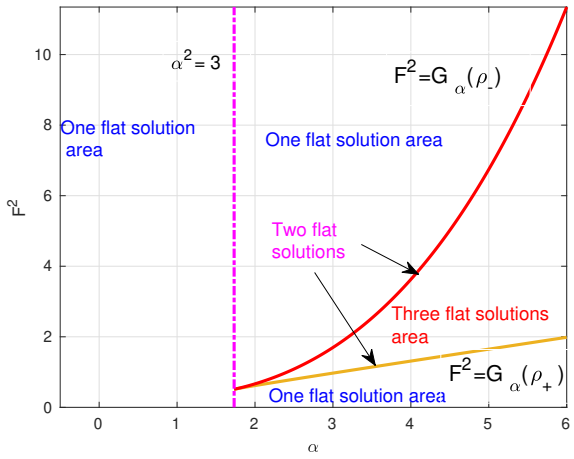

FIG. 1. Number of flat solutions to the LLE depending on the values of the parameters (α, F^2) for $\sigma = 1$.

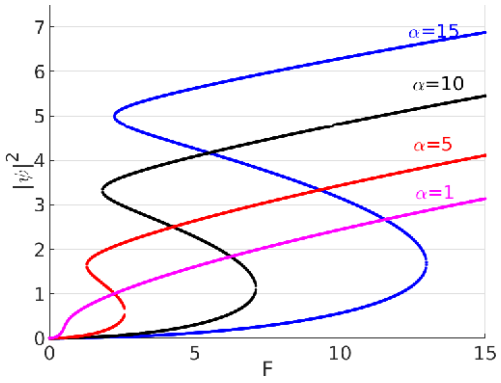

FIG. 2. Variation of $\rho_\bullet = |\psi_\bullet|^2$ as a function of F for $\alpha \in \{1, 5, 10, 15\}$ and $\sigma = 1$.

depicted the variation of $\rho_\bullet = |\psi_\bullet|^2$ as a function of α for various values of F.

As a last remark, let us mention that when the nonlinear part of the LLE is handled through a linearization process, one can easily show that the resulting linear ODE problem has a *unique* solution that is a flat solution. This helps understanding the special role of flat solutions for the LLE.

II.4. Properties of FP-LLE steady state solutions

We have several noticeable results for solutions to the steady state FP-LLE (5) considered here in its equivalent form (6) that extend the results of [17] for RS-LLE.

Proposition 1. *Any solution $\psi = u_1 + \mathrm{i}u_2$ to the steady state FP-LLE (5) satisfies the energy estimate*

$$\|\psi\| \leq \sqrt{2\pi} F.$$

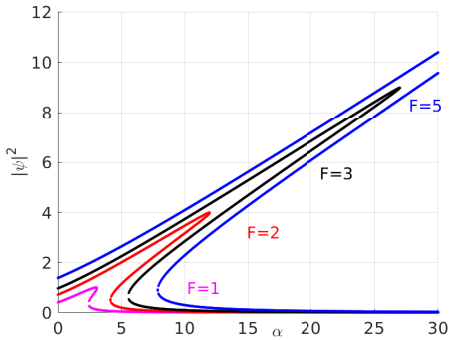

FIG. 3. Variation of $\rho_\bullet = |\psi_\bullet|^2$ as a function of α for $F \in \{1, 2, 3, 5\}$ and $\sigma = 1$.

Moreover, $\int_{-\pi}^{\pi} u_1(\theta)\, \mathrm{d}\theta > 0$.

Proof. This is a direct consequence of the energy estimate (4) for steady state solutions to the FP-LLE. The statement $\int_{-\pi}^{\pi} u_1(\theta)\, \mathrm{d}\theta > 0$ is a direct consequence of relation (A2) in Appendix A. □

Proposition 2. *Any solution ψ to the steady state LLE (5) satisfies*

$$\|\psi\|_\infty \stackrel{\text{def}}{=} \sup_{\theta\in\mathbb{T}} |\psi(\theta)| \leq F + \frac{24\,\pi^2}{|\beta|} F^3.$$

Proof. For the RS-LLE ($\sigma = 0$), this estimate is proved in [17, Section 3]. It does not rely on the detuning parameter. So, it remains valid for any value of this parameter. As a consequence, the estimate is also true for the FP-LLE ($\sigma = 1$), see Remark 1. □

An important feature of the steady state LLE (5) is that for β and F fixed, outside a given range of values for α, the only solutions are flat solutions as stated in Proposition 3 below.

Proposition 3. *There exist $\alpha_\sigma^\star > 0$ and $\alpha_{\sigma\star} < 0$, only dependent on the parameters F and β, such that if $\mathrm{sign}(-\beta)\ \alpha \notin [\alpha_{\sigma\star}, \alpha_\sigma^\star]$ then any steady state solution to the LLE (5) is a flat solution.*

Proof. For the RS-LLE ($\sigma = 0$), this result is obtained directly from [17, Theorem 1.2]. We can deduce the property for the steady state solutions ψ to the FP-LLE from the RS-LLE case as follows. As stated in Remark 1, the FP-LLE can be recast into a RS-LLE with a detuning parameter $\alpha_{RS} = \alpha - \frac{1}{\pi}\|\psi\|^2$ and therefore we can state that if $\mathrm{sign}(-\beta)\left(\alpha - \frac{1}{\pi}\|\psi\|^2\right) \notin [\alpha_{0\star}, \alpha_0^\star]$ then ψ is a flat solution. Thanks to the energy estimate of Proposition 1, we deduce that

- if $\beta < 0$ and for $\alpha < \alpha_{0\star}$ or $\alpha > \alpha_0^\star + 2F^2$
- if $\beta > 0$ and for $\alpha < -\alpha_{0\star}$ or $\alpha > 2F^2 - \alpha_0^\star$

any stationary solution to the FP-LLE is a flat solution. We can merge the two cases as : if $\mathrm{sign}(-\beta)\ \alpha \notin [\alpha_{1\star}, \alpha_1^\star]$ then any stationary solution to the FP-LLE is a flat solution, where we have set $\alpha_{1\star} = \alpha_{0\star}$ and $\alpha_1^\star = \alpha_0^\star + 2F^2$ if $\beta < 0$ and $\alpha_{1\star} = \alpha_{0\star} - 2F^2$ and $\alpha_1^\star = \alpha_0^\star$ if $\beta > 0$. □

Note that explicit bounds for quantities $\alpha_{0\star}$ and $\alpha_0^\star$ can be found in [17].

III. SOME NUMERICAL METHODS FOR SOLVING FP-LLE

In this section, we describe three complementary numerical methods. We start by presenting a Split-Step method to solve the dynamic FP-LLE (1), then we present a Collocation method aimed at solving the steady state FP-LLE (5). Finally, in order to uncover in a more systematic way branches of non constant steady state solutions, we present a continuation method according to the parameter F or α.

III.1. Symmetric Split-Step method

An elementary idea to investigate Kerr frequency combs consists in solving the time-dynamic FP-LLE (1) and observing the solution on a long time scale. Here we choose the Split-Step method. The principle of the Split-Step method is to introduce a subdivision of the time interval and over each sub-interval to solve in a prescribed order the linear and the non-linear parts of the FP-LLE (1a), each of the resulting sub-problem being simpler to solve. Thus, for $t > 0$ fixed, let us consider the linear operator

$$\mathcal{D} : \psi(\cdot,t) \longmapsto -\mathrm{i}\frac{\beta}{2}\,\frac{\partial^2\psi}{\partial\theta^2}(\cdot,t) - (1+\mathrm{i}\alpha)\,\psi(\cdot,t) + F$$

and the non-linear operator

$$\mathcal{N} : \psi(\cdot,t) \longmapsto \mathrm{i}\,\psi(\cdot,t)\left(|\psi(\cdot,t)|^2 + \frac{\sigma}{\pi}\int_{-\pi}^{\pi}|\psi(\zeta,t)|^2\,\mathrm{d}\zeta\right)$$

so that with these notations, the FP-LLE (1a) reads $\frac{\partial}{\partial t}\psi(\cdot,t) = \mathcal{D}\,\psi(\cdot,t) + \mathcal{N}(\psi(\cdot,t))$. Moreover, let us consider a subdivision $(t_k)_{k\in\{0,\dots,K\}}$ of the time interval $[0,T]$ and let $t_{k+\frac{1}{2}} = t_k + \frac{h_k}{2}$ where $h_k = t_{k+1} - t_k$ is the current step-size. The Symmetric Split-Step method consists in solving over each sub-interval $[t_k, t_{k+1}]$, the following three nested problems with space variable θ as a parameter:

$$\begin{cases} \dfrac{\partial}{\partial t}u_k(t) = \mathcal{N}(u_k(t)) & \forall t \in [t_k, t_{k+\frac{1}{2}}] \\ u_k(t_k) = \psi_k \end{cases} \tag{16a}$$

where for $k = 0$, ψ_0 is the initial data and for $k \geq 1$, ψ_k represents the approximated solution at grid point t_k computed at the previous step;

$$\begin{cases} \dfrac{\partial}{\partial t}v_k(t) = \mathcal{D}\,v_k(t) & \forall t \in [t_k, t_{k+1}] \\ v_k(t_k) = u_k(t_{k+\frac{1}{2}}) \end{cases} \tag{16b}$$

where $u_k(t_{k+\frac{1}{2}})$ represents the solution to problem (16a) at half grid point $t_{k+\frac{1}{2}}$;

$$\begin{cases} \dfrac{\partial}{\partial t}w_k(t) = \mathcal{N}(w_k(t)) & \forall t \in [t_{k+\frac{1}{2}}, t_{k+1}] \\ w_k(t_{k+\frac{1}{2}}) = v_k(t_{k+1}) \end{cases} \tag{16c}$$

where $v_k(t_{k+1})$ represents the solution to problem (16b) at node t_{k+1}. An approximated solution to the FP-LLE (1a) at grid node t_{k+1} is then given by

$$\psi(t_{k+1}) \approx w_k(t_{k+1}) \overset{\mathrm{def}}{=} \psi_{k+1}.$$

The efficiency of the Symmetric Split-Step method to solve the FP-LLE (1) relies on the fact that both the linear and non-linear problems in the above splitting can be solved easily. Namely, on the one hand, the solution to problem (16b) can be computed by using the Fourier approach and we get the following explicit formula

$$v_k(t_{k+1}) = \frac{\mathrm{e}^{h_k(1+\mathrm{i}\alpha)} - 1}{1+\mathrm{i}\alpha}\,F + \sum_{n\in\mathbb{Z}}\mu_n\,\mathrm{e}^{d_n h_k}\,\mathrm{e}^{\mathrm{i}n\theta} \tag{17}$$

where the μ_n are the Fourier coefficients of the 2π-periodic function $u_k(t_{k+\frac{1}{2}})$ and $d_n = \mathrm{i}\frac{\beta}{2}n^2 - (1+\mathrm{i}\alpha)$. On the other hand, the solution to problem (16a) can be computed analytically from the following integral representation form:

$$u_k(t) = \psi_k\ \exp\left(\mathrm{i}\int_{t_k}^{t}|u_k(\tau)|^2 + \tfrac{\sigma}{\pi}\|u_k(\tau)\|_0^2\,\mathrm{d}\tau\right). \tag{18}$$

By multiplying each side of the ODE in (16a) by $\overline{u_k}(t)$ and adding it to the complex conjugate equation deduced from (16a), which has been previously multiplied by $u_k(t)$, we can show that $\frac{\partial}{\partial t}|u_k(t)|^2 = 0$. As a consequence $|u_k(t)|^2$ does not depend on t and therefore we have the following explicit expression for the solution deduced from (18):

$$u_k(t) = \psi_k\ \exp\left(\mathrm{i}\,(t-t_k)\big(|\psi_k|^2 + \tfrac{\sigma}{\pi}\|\psi_k\|_0^2\big)\right).$$

A similar expression holds for the solution to (16c) with ψ_k changed for $v_k(t_{k+1})$.

We have developed a free open-source program under MATLAB that solves the time-dynamic FP-LLE (1) by the Split-Step method described here, see [3].

The main drawbacks of this numerical approach is that depending on the initial data ψ_0 in (1d) it may or may not exist a steady state solution to problem (1) and even when the solution is stationary for the choice made for ψ_0, it is not obvious to be sure that a steady state has been reached at the end of the simulation. Moreover,

as usually for such an explicit numerical scheme for a wave-type equation a numerical stability condition (CFL like condition) that links the time step-size to the space step-size exists and imposes to carefully chose the time step-size according to the space step-size [14]. However, this simulation approach is very efficient in terms of computational cost and our working experience has shown that with appropriately manufactured initial data ψ_0, it is possible to obtain a large variety of steady state solutions to the FP-LLE problem.

III.2. A Collocation method

Another way to compute an approximate solution to the steady-state FP-LLE (5) is to use a collocation approach where basically a subdivision of the interval $[-\pi, \pi]$ is introduced leading to a non-linear system of algebraic equations resulting from the boundary conditions and the collocation conditions imposed at the internal nodes of the subdivision. The collocation conditions can be obtained in various way from ODE (5a). An elementary way is to use a finite difference approximation at the nodes of the subdivision $(\theta_n)_{n=0,\dots,N}$ with constant step-size $h = 2\pi/N$ such that $\theta_n = -\pi + n\,h$. At each node θ_n of the subdivision, we approximate the second order derivative $u_k''(\theta_n)$, $k = 1, 2$, in (6a) – (6b) by a centered finite difference formula:

$$u_k''(\theta_n) \approx \frac{u_k(\theta_{n+1}) - 2u_k(\theta_n) + u_k(\theta_{n-1})}{h^2} \tag{19}$$

As well known this approximation formula is second order accurate with respect to the step-size h. Moreover, we can approximate the integral $\mathcal{I}(u_1, u_2)$ from the values of u_k at the subdivision nodes by using the trapezoidal rule that reads, due to the periodic boundary conditions,

$$\mathcal{I}(u_1, u_2) \approx h \sum_{n=1}^{N} \Big(u_1^2(\theta_n) + u_2^2(\theta_n) \Big). \tag{20}$$

It is well known that the trapezoidal quadrature formula has super-convergence properties when applied to the computation of the integral of a smooth periodic function over a period [22].

Denoting by $u_{k,n}$, $n = 0, \dots, N$, the approximate value of $u_k(\theta_n)$, we are led to the set of non-linear equations for $n = 1, \dots, N$

$$\begin{aligned} &-\frac{1}{2}\beta\,\frac{u_{1,n+1} - 2u_{1,n} + u_{1,n-1}}{h^2} - \alpha u_{1,n} - u_{2,n} \\ &+ u_{1,n}\left(u_{1,n}^2 + u_{2,n}^2\right) + \frac{\sigma\,h}{\pi}\,u_{1,n} \sum_{p=1}^{N} \left(u_{1,p}^2 + u_{2,p}^2\right) = 0 \end{aligned} \tag{21a}$$

$$\begin{aligned} &-\frac{1}{2}\beta\,\frac{u_{2,n+1} - 2u_{2,n} + u_{2,n-1}}{h^2} - \alpha\,u_{2,n} + u_{1,n} \\ &+ u_{2,n}\left(u_{1,n}^2 + u_{2,n}^2\right) + \frac{\sigma\,h}{\pi}\,u_{2,n} \sum_{p=1}^{N} \left(u_{1,p}^2 + u_{2,p}^2\right) = F \end{aligned} \tag{21b}$$

Additionally, we have the relation

$$u_{k,N} = u_{k,0} \qquad \forall k = 1, 2 \tag{22}$$

deduced from the periodic boundary condition (6d). Denoting by $U = \left(u_{1,1}, \dots, u_{1,N}, u_{2,1}, \dots, u_{2,N}\right)^\top \in \mathbb{R}^{2N}$ the vector of unknowns, we deduce from (21)–(22) the following non-linear system of $2N$ equations

$$\mathrm{M}\,U + \mathcal{N}(U) = 0 \tag{23}$$

where $\mathrm{M} \in \mathcal{M}_{2N}(\mathbb{R})$ is the block matrix given by

$$\mathrm{M} = \begin{pmatrix} \frac{\beta}{2h^2}\,\mathrm{A} - \alpha\,\mathrm{I}_N & -\mathrm{I}_N \\ \mathrm{I}_N & \frac{\beta}{2h^2}\,\mathrm{A} - \alpha\,\mathrm{I}_N \end{pmatrix} \tag{24}$$

where I_N refers to the identity matrix in $\mathcal{M}_N(\mathbb{R})$ and A is the matrix in $\mathcal{M}_N(\mathbb{R})$ defined as

$$\mathrm{A} = \begin{pmatrix} 2 & -1 & 0 & \cdots & 0 & -1 \\ -1 & 2 & -1 & 0 & \cdots & 0 \\ 0 & \ddots & \ddots & \ddots & & \vdots \\ \vdots & & \ddots & \ddots & \ddots & 0 \\ 0 & & & -1 & 2 & -1 \\ -1 & 0 & \cdots & 0 & -1 & 2 \end{pmatrix}. \tag{25}$$

The non-linear term is defined as

$$\mathcal{N}(U) = \begin{pmatrix} u_{1,1}\left(u_{1,1}^2 + u_{2,1}^2\right) \\ \vdots \\ u_{1,N}\left(u_{1,N}^2 + u_{2,N}^2\right) \\ u_{2,1}\left(u_{1,1}^2 + u_{2,1}^2\right) \\ \vdots \\ u_{2,N}\left(u_{1,N}^2 + u_{2,N}^2\right) \end{pmatrix} + \frac{\sigma\,h}{\pi}\|U\|^2\,U - \begin{pmatrix} 0 \\ \vdots \\ 0 \\ F \\ \vdots \\ F \end{pmatrix} \tag{26}$$

where $\|U\|^2 = U^\top\,U$. Finally, we obtain the approximate solution to the LLE-FP (6) by solving the non-linear system (23) by a Newton solver.

The difficulty in using a Collocation method for solving the FP-LLE (5) comes from the non-uniqueness of its solutions and the high dependence on the initial guess of Newton iterative algorithm on the convergence properties and on the computed solution. In practice, our working experience shows that it is not at all easy to find an initial guess leading to the computation of a steady state solution different from a flat solution. Nevertheless, the method can be very efficient when some prior information is available to design a suitable initial guess.

Note that these difficulties are not specific to the Collocation method presented here. We have also developed a free open-source MATLAB toolbox that uses the alternative Collocation method implemented in MATLAB solver `bvp4c`, see [4]. This Collocation method is based on a three-stage Lobatto formula [21] and the same phenomena were observed.

III.3. Pseudo-arclength continuation method

The above mentioned numerical issues and the wish to have a global picture of steady state solutions led us

as in [17] to investigate Kerr frequency combs generation through a pseudo-arclength continuation method [1]. In the sequel we will denote by λ one of the two parameters F or α chosen as continuation parameter. For ease of exposition, we consider the discrete version of the steady state FP-LLE obtained in Section III.2 expressed in the form of the non-linear system $\mathrm{M}\,U+\mathcal{N}(U)=0$, see (23). Note that a development similar to the one presented here can be done with equations (6a) – (6b) discretized by the Finite Element Method.

We introduce the mapping

$$G_h : (U,\lambda) \in \mathbb{R}^{2N}\times\mathbb{R} \longmapsto \mathrm{M}\,U+\mathcal{N}(U) \in \mathbb{R}^{2N} \quad (27)$$

so that solving the non-linear system (23) amounts to look for (U,λ) such that $G_h(U,\lambda)=0$. As stated before and illustrated in Section IV, solving the non-linear system (23) by a Newton like solver is very dependent on the initial guess used for Newton iterations. To overcome this difficulty, one can use a continuation method. The idea behind the *natural parameter continuation* method is to start from a known solution $(U^{[0]},\lambda^{[0]})$ and to compute a solution to the non-linear system (23) for a parameter value $\lambda^{[1]}=\lambda^{[0]}+\delta\lambda$ for a small increment $\delta\lambda$ by Newton method with initial guess $U^{[0]}$. The solution $U^{[1]}$ provided by Newton method for the parameter value $\lambda^{[1]}$ is then used as an initial guess for Newton method applied to the solving of system (23) for the new parameter value $\lambda^{[2]}=\lambda^{[1]}+\delta\lambda$. And this process is continued by incrementing the value of λ step by step. Such an approach is justified by the *Implicit Function Theorem* (IFT). According to the IFT if $(U^{[0]},\lambda^{[0]})$ is a solution to the non-linear system (23) and $\partial_U G_h(U^{[0]},\lambda^{[0]})$ is not singular, then there exists a unique mapping g from $]\lambda^{[0]}-\varepsilon,\lambda^{[0]}+\varepsilon[$ onto the open ball $B(U^{[0]},r)$ such that the set of solutions to equation $G_h(U,\lambda)=0$ near $(U^{[0]},\lambda^{[0]})$ is a $\mathcal{C}^1$ curve given by $\{(\lambda,g(\lambda))\ ;\ \lambda\in]\lambda^{[0]}-\varepsilon,\lambda^{[0]}+\varepsilon[\}$ with $U^{[0]}=g(\lambda^{[0]})$.

We denote by $\partial_U G_h$ the Jacobian of G_h with derivatives taken with respect to the variable U only. A simple calculation shows that

$$\partial_U G_h(U,\lambda) = \mathrm{M}+\mathrm{J}(U)+\frac{\sigma\,h}{\pi}\left(\left(U^\top U\right)\,\mathrm{I}_{2N}+2\,U\,U^\top\right) \quad (28)$$

where $\mathrm{J}(U)$ is the symmetric block-matrix

$$\mathrm{J}(U)=\begin{pmatrix} J_{11} & J_{12}\\ J_{12} & J_{22}\end{pmatrix}\in\mathcal{M}_{2N}(\mathbb{R})$$

and J_{11}, J_{21}, J_{22} are three diagonal matrices in $\mathcal{M}_N(\mathbb{R})$ with entries

- $3u_{1,n}^2+u_{2,n}^2,\ \ n=1,\dots,N$ for J_{11}
- $2u_{1,n}u_{2,n},\ \ n=1,\dots,N$ for J_{12}
- $u_{1,n}^2+3u_{2,n}^2,\ \ n=1,\dots,N$ for J_{22}.

For the study of the FP-LLE, the idea is to consider for $(U^{[0]},\lambda^{[0]})$ a flat solution since they are explicitly known, see Section II.3. By the continuation method, we can construct from step to step the curve of flat solutions when the parameter λ increases. This has no interest (since flat solutions are explicitly known and do not require a numerical computation) until we reach a point (U,λ) where the assumptions of the IFT are violated, in particular when $\partial_U G_h(U,\lambda)$ is singular. In such a *singular point*, another branch of solutions can bifurcate from the curve of flat solutions and we can use the same continuation method to follow step by step this new curve of steady state solutions.

The singular points along the curve of flat solutions can be calculated explicitly both when considering the steady-state FP-LLE (5) and the discretized problem $G_h(U,\lambda)=0$ (27), as detailed in Appendix B. A necessary condition for a bifurcation to non constant steady state solutions, is given for FP-LLE (5) by the dispersion relation

$$\exists k\in\mathbb{N}^* \quad \frac{1}{\beta}\left(\alpha-2\rho_\bullet(\sigma+1)\pm\sqrt{\rho_\bullet^2-1}\right)=\frac{k^2}{2}. \quad (29)$$

In that case, bifurcation points (BP) are such that $\rho_\bullet\geq 1$. If we choose F as continuation parameter for a fixed value of α, we deduce from (29) that BP on the flat solutions curve are given by $\rho_\bullet$ root of the polynomial of degree 2

$$(4(\sigma+1)^2-1)\,X^2-4(\sigma+1)\left(\alpha-\tfrac{1}{2}\beta k^2\right)X+\left(\alpha-\tfrac{1}{2}\beta k^2\right)^2+1.$$

Let $\Delta_{\mathrm{BP}}(k)=\left(\alpha-\frac{1}{2}\beta k^2\right)^2-(4(\sigma+1)^2-1)$. When $\Delta_{\mathrm{BP}}(k)\geq 0$, the BP are given by

$$\rho_\bullet=\frac{2(\sigma+1)\left(\alpha-\frac{1}{2}\beta k^2\right)\pm\sqrt{\Delta_{\mathrm{BP}}(k)}}{(4(\sigma+1)^2-1)}. \quad (30)$$

Thus, BP along the flat solutions curve can be obtained by computing the values $\rho_\bullet$ given by (30) larger than 1 when the integer k varies in $\mathbb{N}^*$ and by using the relation

$$F=\sqrt{\left(1+(\alpha-(1+2\sigma)\rho_\bullet)^2\right)\rho_\bullet}$$

deduced from (8). Moreover, pursuing the study on the condition on k for which $\rho_\bullet\geq 1$, one can show that when $\beta<0$, we have an infinite number of BP whereas on the contrary when $\beta>0$, we have an finite number of BP.

When the continuation parameter is α and F is fixed, calculations of the BP are a little bit more tricky since in equation (29), α is a function of $\rho_\bullet$ given by (see (8))

$$\alpha=(1+2\sigma)\,\rho_\bullet\pm\sqrt{F^2/\rho_\bullet-1} \quad (31)$$

In particular, BP occur only for $F^2\geq\rho_\bullet\geq 1$. By the change of variable $\rho_\bullet=\frac{F^2}{1+r^2}$, we find that $|r|$ is a root of the polynomial of degree 4

$$P_\pm=4X^4\pm 4\beta k^3\,X^3+(\beta^2k^4+8)\,X^2\pm(4\beta k^2+8F^2)\,X + \beta^2k^4+4\beta k^2F^2+4 \quad (32)$$

where P_+ is related to the $+$ case in relation (31) and P_- is related to the $-$ case. One can see that $P_+(-X) = P_-(X)$ so that the roots of P_- are the opposite of the roots of P_+. Moreover, studying conditions at which the solution $\rho_\bullet$ to (29)–(31) belongs to $[1, F^2]$ makes it possible to show that whatever is the sign of β, the number of BP along the curve of flat solutions when α is the continuation parameter is finite.

The continuation method outlined here has been implemented to deal with a wide variety of equations in the MATLAB Toolbox `pde2path` [23] and we have used it to compute the branches of steady state solutions to the FP-LLE that bifurcate from the curve of flat solutions when either F or α is used as a bifurcation parameter. Illustrations are provided in Section IV.

IV. NUMERICAL ILLUSTRATIONS

To illustrate various properties of the numerical methods, we now present numerical simulations. We focus the presentation on the FP-LLE for the parameter values $\beta = -0.2$ and $F = 1.6$ in order to compare with results obtained in [17] for the RS-LLE. Similar comments to those made with this particular setting could be made with other parameter values. Additional numerical experiments can be undertaken thanks to the open-sources codes [3; 4; 23].

IV.1. Bifurcation diagram for $\beta = -0.2$ and $F = 1.6$

As an example illustrating the continuation method, using `pde2path` [23], we consider the case of the FP-LLE where $\beta = -0.2$, $F = 1.6$ and α is the bifurcation parameter. Note that the choice of the laser pump phase detuning parameter α as a continuation parameter matches well with the experimental use of the FP cavity to generate Kerr frequency combs by tuning step-by-step this parameter. The number of BP along the curve of constant solutions is finite and equal to 14. The BP computed by looking for the roots of the polynomial defined in (32) and by using relation (31) are displayed in Table I with the corresponding value of k in equation (32) (or equivalently in equation (29)). These BP and the branches that bifurcate from the curve of flat solutions at BP are depicted in Fig. 4 where the x-axis shows the bifurcation parameter α and the y-axis shows the $\mathbb{L}^2$ energy norm of the solution defined in (2). The shape of the curve of flat solutions represented in black is typical as shown in Fig. 3. The bifurcation diagram has been obtained using a Finite Difference discretization of the interval $[-\pi, \pi]$ with $N = 2000$ nodes. In Fig. 4, the crossing of two solution curves does not mean that the two solutions are the same at the intersection point but only that the two solutions have the same $\mathbb{L}^2$ norm. By choosing a different norm for the y-axis, one would obtain a different picture of the bifurcation diagram.

ℓ	k	α	ℓ	k	α
1	5	1.87547953318	2	4	2.53835192735
3	6	3.97283765189	4	3	4.99011120397
5	7	7.14357727273	6	2	7.22722777127
7	7	7.69354056103	8	1	7.70074166946
9	6	6.8724727121	10	5	5.92544898526
11	4	5.20621519366	12	3	4.72595101432
13	2	4.44909864888	14	1	4.32300480018

TABLE I. Bifurcation points (BP) on the curve of flat solutions for $\beta = -0.2$ and $F = 1.6$. The label ℓ refers to the position of the BP on the bifurcation diagram depicted on Fig. 4 and k is the integer in the dispersion relation (29).

From the bifurcation diagram in Fig. 4, we can understand the reasons why solving the steady state FP-LLE by a Collocation method for a given set of LLE parameters (β, α, F) is not easy. For instance, one can see on Fig. 4 that for the chosen values of β and F ($\beta = -0.2$ and $F = 1.6$), we have for the value $\alpha = 6$ at least 8 steady state solutions in addition to the three flat solutions (consider the intersections of the vertical line $\alpha = 6$ with the curves of solutions and observe that the branches related to BP with $\ell = 10$, 11 and 13 have a cusp and cross two times the line $\alpha = 6$). Note that the actual number of steady state solutions is probably higher since we have only represented here the branches of solutions that bifurcate from the curve of flat solutions while other branches are likely to bifurcate from the branches issued from the flat solutions curve. Moreover, one can see from the bifurcation diagram shown at the bottom of Fig. 4 that the shape of the bifurcation lines can be rather complicated.

The comparison of the bifurcation diagram in Fig. 4 for the FP-LLE ($\sigma = 1$) to Fig. 5 in [17] that represents the bifurcation diagram for the RS-LLE ($\sigma = 0$) for the same set of parameters ($\beta = -0.2$, $F = 1.6$) highlights similarities and differences between the two kinds of resonators. For instance, one can see that the general shape of the bifurcation diagrams is similar and that the number of BP is the same. This can be explained in view of Remark 1 p. 3. Yet, we can see that with a FP-resonator the range of value for α for which there exist steady state solutions other than flat solutions is wider than this range for a RS-resonator. For a RS-resonator, outside the interval $[-0.5, 3.5]$ for α, we only have flat solutions whereas this interval is $[1.5, 8]$ for a FP-resonator. This observation is in accordance with Proposition 3.

From the steady-state solutions computed by `pde2path`, we can represent the corresponding Kerr frequency comb. For instance, we have depicted in Fig. 5 five steady state solutions and Kerr frequency combs for the FP-LLE parameters $\beta = -0.2$, $F = 1.6$ and $\alpha = 6$. Namely, we have depicted the real, imaginary parts and modulus of the solution ψ as well as the corresponding frequency comb obtained as the sequence $10 \log_{10}(|c_n|^2)$ where $(c_n)_{n\in\mathbb{Z}}$ are the Fourier coefficients of ψ.

We want to point out that the continuation method provides a thorough knowledge of steady state solutions to the FP-LLE but this requires a long computation

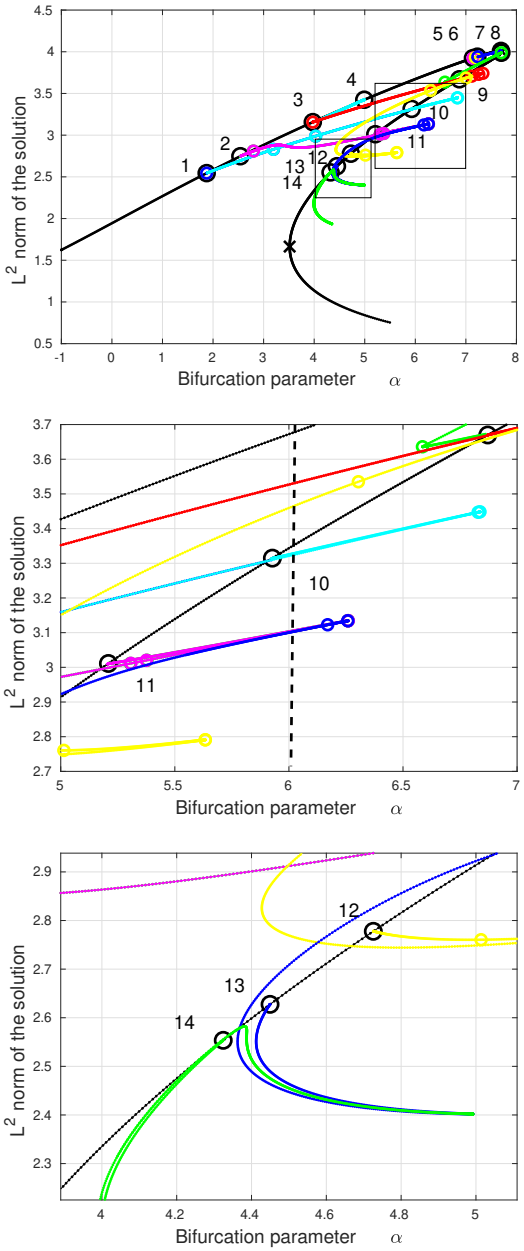

FIG. 4. Bifurcation diagram. Integers refer to the label ℓ of the BP as given in Table I. Top: BP (black circle) on the curve of flat solutions (black curve) for $\beta = -0.2$ and $F = 1.6$ and branches of solutions bifurcating from the BP (color curves). Middle: Zoom on the bifurcation diagram of the larger rectangle area where the bifurcation curves cross the line $\alpha = 6$. Bottom: Zoom on the bifurcation diagram corresponding to the smaller rectangle area.

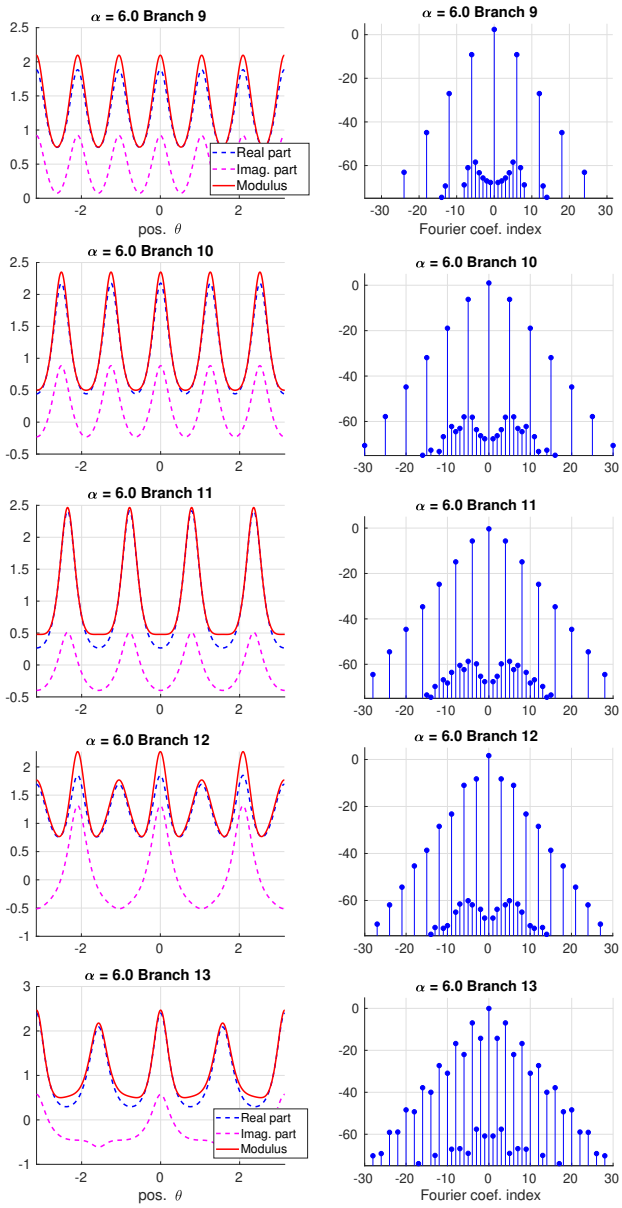

FIG. 5. Solutions to the FP-LLE for $\alpha = 6, \beta = -0.2$ and $F = 1.6$ (left) and corresponding Kerr frequency combs (right) obtained on the bifurcation branches starting from BP 9, 10, 11, 12 and 13 (from top to bottom). On the left, the real part of the solution is drawn in blue dashed line, its imaginary part in magenta dashed line and it modulus in red solid line. The frequency comb on the right is a representation of the sequence $10\log_{10}(|c_n|^2)$ where $(c_n)_{n\in\mathbb{Z}}$ are the Fourier coefficients of the solution.

time. For instance, obtaining the bifurcation diagram in Fig. 4 required several hours of computation on a computer work-station. Moreover, depending on the parameter values it can be difficult to interpret the bifurcation diagram.

IV.2. Solutions to the dynamic LLE for $\beta = -0.2$, $F = 1.6$ and $\alpha = 6$

Let us now consider the Split-Step method presented in Section III.1 and implemented in MATLAB Toolbox `S3F4LLE` [3] to solve the time-dynamic FP-LLE (1). From the physics point of view, a precise knowledge of the initial state of the FP cavity (described by the function ψ_0

in the initial condition (1d)) is merely impossible and for the purpose of numerical simulation, we have to make the choice of manufactured initial conditions. Let us consider for instance an initial condition corresponding to a finite lattice sum of Gaussian functions

$$g_{m,P}(\theta) = \sum_{p=-P}^{P} \sum_{\ell=1}^{m} \mathrm{e}^{-\frac{1}{|\beta|}\left(\theta+2p\pi+\frac{2\ell-m-1}{m}\pi\right)^2}. \qquad (33)$$

Here the main parameter is the integer m aimed at exciting frequency combs of width $k = m$. The integer parameter P allows, function of the value of β, a precise approximation of exact periodicity at $\theta = \pm\pi$.

We consider some of the solutions corresponding to the bifurcation diagram depicted in Fig. 4. We have depicted in Fig. 6 the time evolution of the solution to the FP-LLE (1) for $\alpha = 6, \beta = -0.2$ and $F = 1.6$ when the initial condition is $\psi_0 = g_{4,2} + \psi_{\bullet,2}$ where $\psi_{\bullet,2}$ denotes the flat solution with intermediate value among the 3 flat solutions of the FP-LLE for this set of parameters. Simulation is carried out until normalized time $T = 100$ with 10^5 sampling points and 2^8 space sampling points for the FFT computations. One can see that after strong variations of the solution over a short duration (less than 10 units of time), the solution converges toward a steady state solution that has the features of the steady state solution observed on branch 11, see Fig. 5. The spacing of the comb teeth is 4 units in accordance with the value of k given in Table I. Compared to the comb depicted in Fig. 5 for branch 11, the pattern at the bottom of the comb in Fig. 6 has disappeared which shows that the bottom pattern is a numerical artifact.

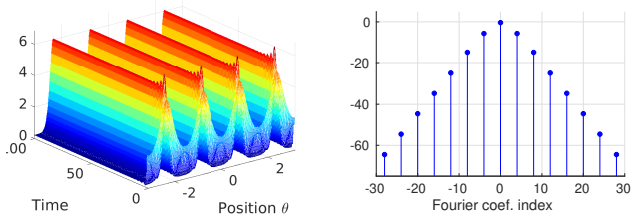

FIG. 6. Left: Time evolution of the square modulus $|\psi|^2$ of the solution ψ to the time-dynamic FP-LLE for $\alpha = 6, \beta = -0.2$ and $F = 1.6$ with initial condition corresponding to a finite lattice sum of Gaussian functions (33) with $P = 2$ and $m = 4$. Right: Corresponding Kerr frequency comb.

Note that not all the steady state solutions computed by the continuation method are stable. The question of the stability of steady state solutions to the RS-LLE ($\sigma = 0$) is investigated from a mathematical point of view in [19]. For illustrative purposes, we have depicted in Fig. 7 the solution to the time dynamic FP-LLE (1) at time 100 with the same set of parameters as those of Fig. 6 excepted that $m = 5$ in the initial condition given by the finite lattice sum of Gaussian functions. One can see that this solution matches well with the steady state solution obtained by the continuation method for $\alpha = 6$ on branch 10, see Fig. 5. However, when the evolution of the solution is observed on a duration of 250 units of time, one can see that it seems to oscillate (or to hesitate) between two shapes (that are very close to each other) but finally around time 210 the solution tends to the smaller of the 3 flat solutions, see Fig. 8. The same observation can be made when using as initial condition the finite lattice sum of Gaussian functions with $m = 3$ or $m = 6$ where the solution firstly look very close to the steady state solution observed on branch 9 before to suddenly change its behavior and to converge to the smaller flat solution.

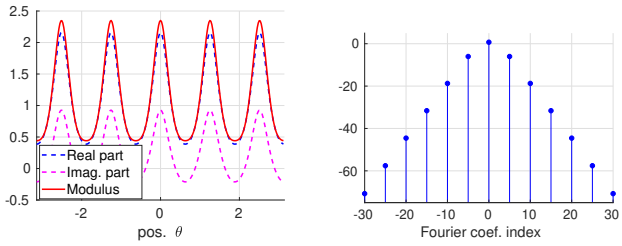

FIG. 7. Left: Solution to the time-dynamic FP-LLE for $\alpha = 6, \beta = -0.2$ and $F = 1.6$ with initial condition corresponding to a finite lattice sum of Gaussian functions with $P = 2$ and $m = 5$ at time 100. Right: Corresponding Kerr frequency comb.

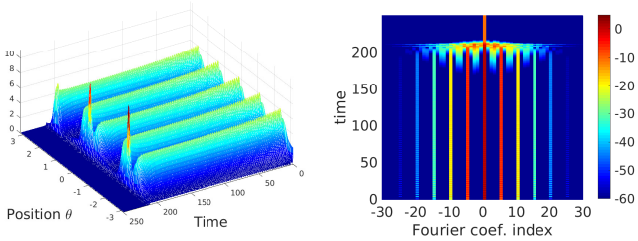

FIG. 8. Left: Time evolution of the square modulus of the solution to the time-dynamic FP-LLE for the parameters of Fig. 7. Right: Variation of the solution spectrum with time.

As a last illustration, let us consider the set of parameters $\beta = -0.2$, $F = 1.6$ and $\alpha = 4$ with initial condition $\psi_0 = g_{6,2} + \psi_{\bullet,2}$ where $\psi_{\bullet,2}$ denotes the flat solution with intermediate value among the 3 flat solutions of the FP-LLE for this set of parameters and $g_{2,2}$ the finite lattice sum of Gaussian functions. We have depicted in Fig. 9 the evolution of the square modulus of the solution with time and we can see four distinct behaviors for the solution from the initial condition to the steady state that appears from time 150. By using the bifurcation diagram given in Fig. 4 and the various solution shapes along the bifurcation branches depicted in Fig. 5, one can infer that the solution has converged to the steady state solution of branch 13. It is also interesting to run a simulation with initial condition $\psi_0 = g_{2,2} + \psi_{\bullet,3}$ where $\psi_{\bullet,3}$ denotes the flat solution with higher value. The evolution of the solu-

tion with time also exhibits four distinct stages but this time the solution converges to the steady state solution of branch 11 as illustrated in Fig. 10. One can note by comparing Fig. 10 and Fig. 9 that when the steady state regime is reached, the two combs are identical and that the two solutions are translated from each other. This observation is in accordance with the remark made in Section II.1 regarding the translation invariance properties of steady state solution.

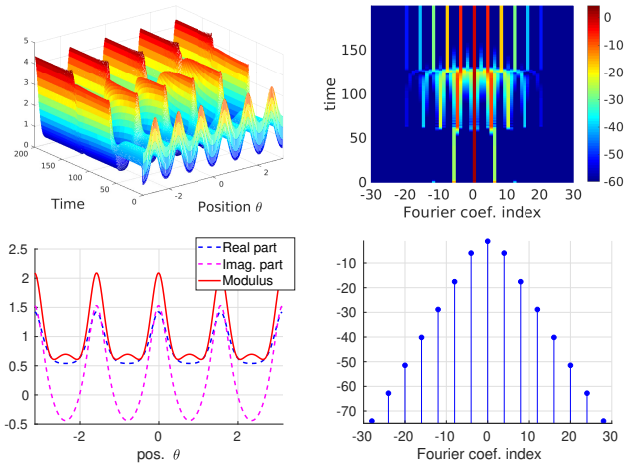

FIG. 9. Top-left: Time evolution of the square modulus of the solution to the time-dynamic FP-LLE for $\beta = -0.2$, $F = 1.6$ and $\alpha = 4$ with initial condition $\psi_0 = g_{6,2} + \psi_{\bullet,2}$. Top-right: Variation of the solution spectrum with time. Bottom-left: Solution at final time $T = 200$. Bottom-right: Kerr frequency comb of the steady state solution.

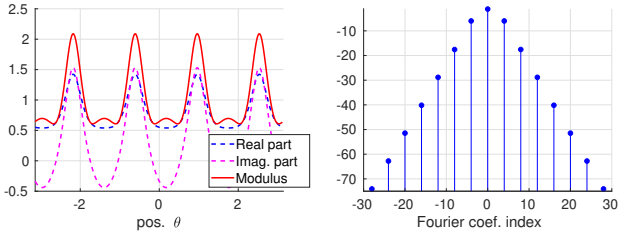

FIG. 10. Left: Solution at time $T = 200$ to the FP-LLE for $\psi_0 = g_{6,2} + \psi_{\bullet,3}$ with other parameters as in Fig. 9. Right: Kerr frequency comb of the steady state solution.

In view of the results presented above, the question of whether a steady state has been obtained or not is major but not easy to answer from the graphical representation of the solution. In order to have a more effective indicator, we propose to compute at each time-step t_n the quantity

$$\mathcal{V}(\psi, t_n) = \max_{\theta\in[-\pi,\pi]} \left| \frac{\psi(\theta, t_n) - \psi(\theta, t_{n-1})}{t_n - t_{n-1}} \right|. \qquad (34)$$

This numerical indicator shows how the computed solution ψ varies from a time-step to the other and therefore, values of $\mathcal{V}(\psi, t_n)$ closed to the machine epsilon indicate that a steady state regime has been reached. We have depicted in Fig. 11 the variations with time of the decimal logarithm of $\mathcal{V}(\psi, t_n)$ for the simulation reported in Fig. 9. One can easily identify the various states the solution goes through in the interval $[0, 150]$ before converging to its final steady state that is fully attained around time 400.

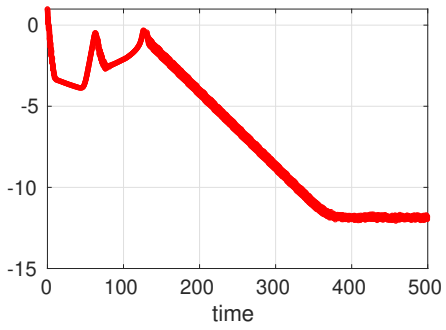

FIG. 11. Variations with time of the decimal logarithm of the indicator $\mathcal{V}(\psi, t_n)$ for the simulation reported in Fig. 9.

To conclude, in connection with Kerr comb generation, we can stress once again the leading role played by the initial data ψ_0 on the type of steady state solution attained (even if no simple rule of thumb can be formulated) and the need of a steady state indicator such as the one defined in (34) to have the assurance that a steady state has been reached when the simulation is ended.

IV.3. Stationary solutions computed by the Collocation method

In [7, Section V], the authors provide an analytical approximate expression for Soliton solution to the FP-LLE. (Note that the use of this expression requires the solving of a non-linear equation and therefore necessitates a numerical solver anyway.) When they exist, Solitons solutions to the FP-LLE can be computed more accurately by the Collocation method described in Section III.2 and implemented in our MATLAB toolbox `COLLE` [4]. For instance we have depicted in Fig. 12 the Soliton solution to the FP-LLE for the values $\beta = -0.02$, $F = \sqrt{3}$ and $\alpha = 4.37$ used in [7], obtained by the Collocation method for an initial guess $\psi_{\bullet,1} + g_{1,4}$ where $\psi_{\bullet,1}$ denotes the flat solution with lower value and $g_{1,4}$ the finite lattice sum of Gaussian functions (33) and a number of discretization nodes $N = 10^3$. The CPU time required for this computation is 9.1 s. The relative error between the approximate analytical expression of the Soliton proposed in [7] and the solution computed by the Collocation method measured in the energy norm is 5.9%.

It is also possible by using the Collocation method to compute solutions to the FP-LLE referred to as Turing patterns in [7, Section VI] and observed for $\beta = -0.02$,

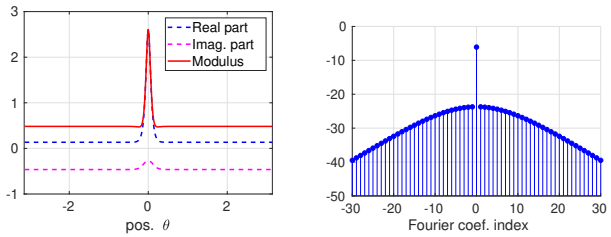

FIG. 12. Left: Soliton solution to the FP-LLE for $\beta = -0.02$, $F = \sqrt{3}$ and $\alpha = 4.37$. Right: Kerr frequency comb of the Soliton.

$F = \sqrt{6}$ and $\alpha = 2.5$. We have depicted in Fig. 13 the solution computed by the Collocation method for an initial guess $\psi_0 : \theta \mapsto \psi_{\bullet,1} + \cos(m\theta)$ for $m = 16$.

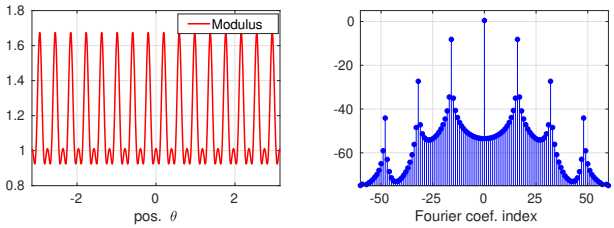

FIG. 13. Left: Turing pattern solution with 16 rolls to the FP-LLE for $\beta = -0.02$, $F = \sqrt{6}$ and $\alpha = 2.5$. Right: Kerr frequency comb of the computed Turing pattern. The main teeth of the comb are located every 16 units.

V. CONCLUSION

We have presented three numerical approaches to study by numerical simulation Kerr frequency combs in optical resonators. We have considered two variants of the Lugiato-Lefever equation (LLE) that were introduced in the literature to model respectively light-wave propagation in ring-shape (RS) resonators and Fabry-Perot (FP) resonators. We have focused our attention on the LLE for FP resonators because this topic has been introduced recently and is presently extensively investigated in optics. The particularity of the FP-LLE compared to the RS-LLE is an additional integral term that makes the LLE non-linearity spatially non-local and consequently makes its numerical resolution more difficult.

The three numerical approaches we have described in the paper include a Split-Step method to solve the time-dynamic FP-LLE and a Collocation method to solve the steady state FP-LLE. These methods are very efficient but the computed solution highly depends on the initial condition when solving the time-dynamic FP-LLE or on the initial guess solution when solving the steady state LLE by the Collocation method and these initial data are not easy to know or to guess. We have pointed out in the paper the specific role played by flat solutions, *i.e.* spatially and temporally constant solutions, and we found that they are the solutions the most often observed during numerical simulations if the initial data has not the specific features to induce convergence to a non-flat steady state solution. In order to overcome this issue, we have presented a continuation method with respect to the parameters α or F of the LLE that exhibits bifurcation branches from flat solutions. We obtain a comprehensive picture of the various solutions to the steady state LLE and this constitutes an important help in the interpretation of the results provided by the Split-Step and the Collocation methods.

The numerical methods presented in this paper to solve the FP-LLE have been implemented under MATLAB and specific toolboxes, distributed as free software [3; 4] have been developed.

ACKNOWLEDGMENTS

This work has been undertaken in the framework of the ANR project ROLLMOPS (optical resonator with ultra-high quality factor for high spectral purity microwave signals generation) funded by the French Agence Nationale de la Recherche (2021-2024).

Appendix A: Energy estimate for the solution to the time dynamic FP-LLE

Let us consider a solution ψ to the time dynamic FP-LLE (1a). By multiplying (1a) by the solution conjugate $\overline{\psi}$ and integrating over $[-\pi, \pi]$, we obtain

$$\int_{-\pi}^{\pi} \partial_t \psi(\theta,t)\,\overline{\psi}(\theta,t)\,\mathrm{d}\theta = -\mathrm{i}\frac{\beta}{2}\int_{-\pi}^{\pi} \partial^2_{\theta\theta}\psi(\theta,t)\,\overline{\psi}(\theta,t)\,\mathrm{d}\theta - (1+\mathrm{i}\alpha)\,\|\psi(t)\|^2 + \mathrm{i}\|\psi^2(t)\|^2 + \mathrm{i}\frac{\sigma}{\pi}\,\|\psi(t)\|^4 + F\int_{-\pi}^{\pi}\overline{\psi}(\theta,t)\,\mathrm{d}\theta. \tag{A1}$$

By using Green Formula and periodic boundary conditions (1b), we obtain

$$\int_{-\pi}^{\pi} \partial^2_{\theta\theta}\psi(\theta,t)\,\overline{\psi}(\theta,t)\,\mathrm{d}\theta = -\int_{-\pi}^{\pi} |\partial_\theta\psi(\theta,t)|^2\,\mathrm{d}\theta.$$

Thus, considering the real part of (A1), we deduce that

$$\frac{1}{2}\frac{\partial}{\partial t}\int_{-\pi}^{\pi}|\psi(\theta,t)|^2\,\mathrm{d}\theta + \|\psi(t)\|^2 = F\int_{-\pi}^{\pi}\mathrm{Re}(\psi)(\theta,t)\,\mathrm{d}\theta \tag{A2}$$

and the Cauchy-Schwarz inequality yields

$$F\int_{-\pi}^{\pi}\mathrm{Re}(\psi)(\theta,t)\,\mathrm{d}\theta \le \pi F^2 + \frac{1}{2}\int_{-\pi}^{\pi}\mathrm{Re}(\psi)^2(\theta,t)\,\mathrm{d}\theta \le \pi F^2 + \frac{1}{2}\|\psi(t)\|^2.$$

We deduce from (A2) that $\frac{\partial}{\partial t}\|\psi(t)\|^2 + \|\psi(t)\|^2 \le 2\pi F^2$ and it follows that

$$\frac{\partial}{\partial t}\left(\mathrm{e}^t\|\psi(t)\|^2\right) \le 2\pi F^2\,\mathrm{e}^t.$$

Finally, integrating this inequality for $t \in [0,T]$, we deduce the following energy estimate for the solution to the FP-LLE:

$$\forall T>0 \quad \|\psi(T)\|^2 \le \mathrm{e}^{-T}\,\|\psi_0\|^2 + 2\pi F^2\,(1-\mathrm{e}^{-T}). \quad \text{(A3)}$$

Appendix B: Singular points on the curve of flat solutions

The steady state FP-LLE can be written as $\mathcal{F}(\psi)=0$ where

$$\mathcal{F}(\psi) = -i\frac{\beta}{2}\partial_{\theta\theta}\psi - (1+i\alpha)\psi + i\psi\Big(|\psi|^2 + \frac{\sigma}{\pi}\|\psi\|^2\Big) + F.$$

A necessary condition for a flat solution $\psi_\bullet$ to be the onset of a bifurcation is that $\partial_\psi\mathcal{F}(\psi_\bullet)$ is not invertible. The search for bifurcation points can be notably simplified, a fact highlighted in [19], if instead of $\mathcal{F}$, one considers the FP-LLE in the form

$$\mathcal{F}_\bullet(v) \stackrel{\text{def}}{=} \psi_\bullet^{-1}\,\mathcal{F}\big(\psi_\bullet(1+v)\big) = 0$$

with v as new unknown. Differentiating $\mathcal{F}_\bullet$ at 0 yields

$$\partial_v\mathcal{F}_\bullet(0) = \psi_\bullet^{-1}\,\partial_\psi\mathcal{F}(\psi_\bullet)\,\psi_\bullet\,.$$

The complex valued operator $\partial_v\mathcal{F}_\bullet(0)$ acts on complex valued functions w. Considering the real and imaginary parts of w and $\partial_v\mathcal{F}_\bullet(0)[w]$, one transforms the expression of $\partial_v\mathcal{F}_\bullet(0)$ into a 2×2 matrix of real valued operator blocks. Considering the column vector $(\mathrm{Im}(\partial_v\mathcal{F}_\bullet(0)[w]), -\mathrm{Re}(\partial_v\mathcal{F}_\bullet(0)[w]))^\top$ as a function of $(\mathrm{Re}\,w, \mathrm{Im}\,w)^\top$, we find that the conditions for non-invertibility of $\partial_\psi\mathcal{F}(\psi_\bullet)$ are given by the non-invertibility of

$$M + J_\bullet + K_\bullet = \begin{pmatrix} \frac{\beta}{2}\mathcal{A} - \alpha\mathbb{I} & -\mathbb{I} \\ \mathbb{I} & \frac{\beta}{2}\mathcal{A} - \alpha\mathbb{I}\end{pmatrix} + \begin{pmatrix} 3\rho_\bullet\mathbb{I} & 0 \\ 0 & \rho_\bullet\mathbb{I}\end{pmatrix} + \begin{pmatrix} 2\sigma\rho_\bullet(\mathbb{I}+\mathcal{I}) & 0 \\ 0 & 2\sigma\rho_\bullet\mathbb{I}\end{pmatrix} \quad \text{(B1)}$$

in which appear the operators $\mathcal{A}: w \mapsto -\partial_{\theta\theta}w$ and $\mathcal{I}: w \mapsto \frac{1}{\pi}\int_{-\pi}^{\pi} w$. Note that M corresponds to the linear part $-i\frac{\beta}{2}\partial_{\theta\theta} - (1+i\alpha)\mathbb{I}$ of $\mathcal{F}$ while $J_\bullet$ and $K_\bullet$ come from the linearization of the cubic parts $\psi \mapsto i\psi|\psi|^2$ and $\psi \mapsto \frac{\sigma}{\pi}i\psi\|\psi\|^2$. Relying on the diagonalization of the operators $\mathcal{A}$ and $\mathcal{I}$ in the trigonometric basis $\cos k\theta$, $k\in\mathbb{N}$, and $\sin k\theta$, $k\in\mathbb{N}^*$, it is straightforward to deduce the block diagonalization $(\widehat{L}_k)_{k\in\mathbb{N}}$ of $M+J_\bullet+K_\bullet$ where

$$\widehat{L}_k = \begin{pmatrix} \frac{\beta}{2}k^2 - \alpha + \rho_\bullet(3+2\sigma) + 4\sigma\rho_\bullet\delta_{0k} & -1 \\ 1 & \frac{\beta}{2}k^2 - \alpha + \rho_\bullet(1+2\sigma)\end{pmatrix} \quad \text{(B2)}$$

from which we find the following dispersion relations necessary to have a bifurcation point at $\psi_\bullet$ (compare with [7, eq. (54)]): $\exists k\in\mathbb{N}$, $\exists\varepsilon\in\{\pm1\}$ such that

$$-\alpha + 2\rho_\bullet(1+2\sigma) = \varepsilon\sqrt{\rho_\bullet^2(1+2\sigma)^2 - 1} \quad \text{if} \quad k=0 \quad \text{(B3)}$$

$$\tfrac{\beta}{2}k^2 - \alpha + 2\rho_\bullet(1+\sigma) = \varepsilon\sqrt{\rho_\bullet^2 - 1} \qquad \text{if} \quad k\neq 0.$$

A similar investigation of necessary conditions for bifurcations from the curve of flat solutions can be achieved for the discrete version (23) of the steady-state FP-LLE. When $U = U_\bullet$ is associated to a flat solution $\psi_\bullet = u_{\bullet,1} + iu_{\bullet,2}$, we have $u_{1,n} = u_{\bullet,1}$ and $u_{2,n} = u_{\bullet,2}$ for all n, and $U^\top U = N(u_{\bullet,1}^2 + u_{\bullet,2}^2) = N\rho_\bullet$. Hence formula (28) becomes

$$\partial_U G_h(U_\bullet,\lambda) = \mathrm{M} + \begin{pmatrix} (3u_{\bullet,1}^2 + u_{\bullet,2}^2)\,\mathrm{I}_N & 2u_{\bullet,1}u_{\bullet,2}\,\mathrm{I}_N \\ 2u_{\bullet,1}u_{\bullet,2}\,\mathrm{I}_N & (u_{\bullet,1}^2 + 3u_{\bullet,2}^2)\,\mathrm{I}_N\end{pmatrix} + 2\sigma\rho_\bullet\,\mathrm{I}_{2N} + \frac{2\sigma}{N}\begin{pmatrix} u_{\bullet,1}^2\,\mathrm{K}_N & u_{\bullet,1}u_{\bullet,2}\,\mathrm{K}_N \\ u_{\bullet,1}u_{\bullet,2}\,\mathrm{K}_N & u_{\bullet,2}^2\,\mathrm{K}_N\end{pmatrix}$$

where M is given by (24), K_N denotes the $N\times N$ matrix with all coefficients 1.

By a pre-multiplication by the matrix P^{-1} and a post-multiplication by the matrix P where

$$\mathrm{P} = \begin{pmatrix} u_{\bullet,1}\,\mathrm{I}_N & -u_{\bullet,2}\,\mathrm{I}_N \\ u_{\bullet,2}\,\mathrm{I}_N & u_{\bullet,1}\,\mathrm{I}_N\end{pmatrix}$$

we obtain that $\partial_U G_h(U_\bullet,\lambda)$ is similar to the matrix

$$\mathrm{M} + \rho_\bullet\begin{pmatrix} 3\,\mathrm{I}_N & 0 \\ 0 & \mathrm{I}_N\end{pmatrix} + \rho_\bullet\begin{pmatrix} 2\sigma\,\mathrm{I}_N & 0 \\ 0 & 2\sigma\,\mathrm{I}_N\end{pmatrix} + \frac{2\sigma}{N}\begin{pmatrix} \rho_\bullet\,\mathrm{K}_N & 0 \\ 0 & 0\end{pmatrix}. \quad \text{(B4)}$$

Note that (B4) is the finite difference discretization of (B1), combined with trapezoidal quadrature formula.

The matrix A given by (25) can be easily diagonalized by noting that it is a circulant matrix with non-zero coefficients $c_0 = 2$, $c_1 = -1$, and $c_{N-1} = -1$. We deduce that its eigenvalues are $\lambda_k = \sum_{j=0}^{N-1} c_j e^{ij\frac{2k\pi}{N}} = 2(1-\cos\frac{2k\pi}{N})$ for $k = 0,\dots,N-1$, associated with eigenvectors $V_k = (1, e^{i\frac{2k\pi}{N}}, \dots, e^{i(N-1)\frac{2k\pi}{N}})^\top$. Noticing that $\lambda_k = \lambda_{N-k}$ for $k = 1,\dots,[\frac{N}{2}]$ and $V_{N-k} = \overline{V}_k$, we find the basis of real eigenvectors $\left(1, \cos\frac{2k\pi}{N}, \dots, \cos(N-1)\frac{2k\pi}{N}\right)^\top$ and $\left(0, \sin\frac{2k\pi}{N}, \dots, \sin(N-1)\frac{2k\pi}{N}\right)^\top$ that correspond to the eigenvectors $\cos k\theta$ and $\sin k\theta$ of $\mathcal{A}$ evaluated at the grid nodes θ_n, $n = 0,\dots,N-1$.

With this information at hand, we find that the matrix given in (B4) is similar to the diagonal matrix with diagonal block given by $(\widehat{L}_{N,k})_{k=0,\dots,[\frac{N}{2}]}$ where

$$\widehat{L}_{N,k} = \begin{pmatrix} \frac{\beta}{2}\,\omega_{N,k} - \alpha + \rho_\bullet(3+2\sigma) + 4\sigma\rho_\bullet\delta_{0k} & -1 \\ 1 & \frac{\beta}{2}\,\omega_{N,k} - \alpha + \rho_\bullet(1+2\sigma)\end{pmatrix}$$

and $\omega_{N,k} \stackrel{\text{def}}{=} \frac{2}{h^2}\,(1-\cos\frac{2k\pi}{N}) = \frac{2}{h^2}\,(1-\cos kh)$. We deduce that necessary conditions for a bifurcation point at $U_\bullet$ are

given by a modification of (B3) in which k^2 is replaced by $\omega_{N,k}$ and $k \leq \frac{N}{2}$. Note that when the step-size h tends to 0, we retrieve from the discrete dispersion relation the continuous dispersion relation (B3).

[1] E. L. Allgower and K. Georg, *Introduction to numerical continuation methods*, Society for Industrial and Applied Mathematics, 2003, https://doi.org/10.1137/1.9780898719154.

[2] S. Balac, *Modeling optical Kerr effect in Fabry-Perot resonators*, tech. report, IRMAR, University of Renness, France, HAL 04481700, https://hal.science/hal-04481700, 2022.

[3] S. Balac, *S3F4LLE: a Matlab solver for the Lugiato-Lefever equation in the dynamic regime*, tech. report, IRMAR, University of Rennes, France, HAL 04662404, https://hal.science/hal-04662404, 2022.

[4] S. Balac, *COLLE : a Matlab toolbox for solving the Lugiato-Lefever equation in the stationary regime*, tech. report, IRMAR, University of Rennes, France, HAL 04318809, https://hal.science/hal-04318809, 2023.

[5] Y. K. Chembo, *Kerr optical frequency combs: theory, applications and perspectives*, Nanophotonics, 5 (2016), pp. 214–230, https://doi.org/doi:10.1515/nanoph-2016-0013, 10.1515/nanoph-2016-0013.

[6] Y. K. Chembo and C. R. Menyuk, *Spatiotemporal lugiato-lefever formalism for Kerr-comb generation in whispering-gallery-mode resonators*, Phys. Rev. A, 87 (2013), p. 053852, https://doi.org/10.1103/PhysRevA.87.053852.

[7] D. C. Cole, A. Gatti, S. B. Papp, F. Prati, and L. Lugiato, *Theory of Kerr frequency combs in Fabry-Perot resonators*, Phys. Rev. A, 98 (2018), p. 013831, https://doi.org/10.1103/PhysRevA.98.013831.

[8] M. G. Crandall and P. H. Rabinowitz, *Bifurcation from simple eigenvalues*, Journal of Functional Analysis, 8 (1971), pp. 321–340, https://doi.org/10.1016/0022-1236(71)90015-2.

[9] M. Dauge, S. Balac, G. Caloz, and Z. Moitier, *Whispering gallery modes and frequency combs: Two excursions in the world of photonic resonators*, in Book of Abstracts, The 16th International Conference on Mathematical and Numerical Aspects of Wave Propagation (WAVES 2024), L. Gizon, ed., Berlin, Germany, June 2024, https://doi.org/10.17617/3.MBE4AA.

[10] L. Delcey and M. Haragus, *Periodic waves of the Lugiato–Lefever equation at the onset of Turing instability*, Phil. Trans. R. Soc. A., (2018), p. 20170188, https://doi.org/http://doi.org/10.1098/rsta.2017.0188.

[11] J.-M. Ghidaglia, *Finite dimensional behavior for weakly damped driven Schrödinger equations*, Annales de l'I.H.P. Analyse non linéaire, 5 (1988), pp. 365–405, https://doi.org/10.1016/S0294-1449(16)30343-2.

[12] C. Godey, *A bifurcation analysis for the Lugiato-Lefever equation*, The European Physical Journal D, 71 (2017), https://doi.org/10.1140/epjd/e2017-80057-2.

[13] C. Godey, I. V. Balakireva, A. Coillet, and Y. K. Chembo, *Stability analysis of the spatiotemporal lugiato-lefever model for Kerr optical frequency combs in the anomalous and normal dispersion regimes*, Phys. Rev. A, 89 (2014), p. 063814, https://doi.org/10.1103/PhysRevA.89.063814.

[14] T. Jahnke, M. Mikl, and R. Schnaubelt, *Strang splitting for a semilinear Schrödinger equation with damping and forcing*, Journal of Mathematical Analysis and Applications, 455 (2017), pp. 1051–1071, https://doi.org/10.1016/j.jmaa.2017.06.004.

[15] J. K. Jang, M. Erkintalo, S. G. Murdoch, and S. Coen, *Writing and erasing of temporal cavity Solitons by direct phase modulation of the cavity driving field*, Opt. Lett., 40 (2015), pp. 4755–4758, https://doi.org/10.1364/OL.40.004755.

[16] L. A. Lugiato and R. Lefever, *Spatial dissipative structures in passive optical systems*, Phys. Rev. Lett., 58 (1987), pp. 2209–2211, https://doi.org/10.1103/PhysRevLett.58.2209.

[17] R. Mandel and W. Reichel, *A priori bounds and global bifurcation results for frequency combs modeled by the Lugiato–Lefever equation*, SIAM Journal on Applied Mathematics, 77 (2017), pp. 315–345, https://doi.org/10.1137/16M1066221.

[18] A. B. Matsko, A. A. Savchenkov, W. Liang, V. S. Ilchenko, D. Seidel, and L. Maleki, *Mode-locked Kerr frequency combs*, Opt. Lett., 36 (2011), pp. 2845–2847, https://doi.org/10.1364/OL.36.002845.

[19] T. Miyaji, I. Ohnishi, and Y. Tsutsumi, *Bifurcation analysis to the Lugiato–Lefever equation in one space dimension*, Physica D: Nonlinear Phenomena, 239 (2010), pp. 2066–2083, https://doi.org/10.1016/j.physd.2010.07.014.

[20] E. Obrzud, S. Lecomte, and T. Herr, *Temporal solitons in microresonators driven by optical pulses*, Nature Photonics, 11 (2017), p. 600–607, https://doi.org/10.1038/nphoton.2017.140.

[21] L. Shampine and J. Kierzenka, *A BVP solver based on residual control and the Matlab PSE*, ACM Trans. Math. Softw., 27 (2001), p. 299–316, https://doi.org/10.1145/502800.502801.

[22] L. N. Trefethen and J. A. C. Weideman, *The exponentially convergent trapezoidal rule*, SIAM Review, 56 (2014), pp. 385–458, https://doi.org/10.1137/130932132.

[23] H. Uecker, *Numerical continuation and bifurcation in nonlinear PDEs*, Society for Industrial and Applied Mathematics, Philadelphia, PA, 2021, https://doi.org/10.1137/1.9781611976618.

[24] Z. Ziani, T. Bunel, A. M. Perego, A. Mussot, and M. Conforti, *Theory of modulation instability in Kerr Fabry-Perot resonators beyond the mean-field limit*, Phys. Rev. A, 109 (2024), p. 013507, https://doi.org/10.1103/PhysRevA.109.013507.